STRONG GROUND MOTION SIMULATION OF THE 2019 JAVA EARTHQUAKE USING EMPIRICAL GREEN'S FUNCTION METHOD

A. Octantyo[(1)], H. Miyake[(2)], T. Yokoi[(3)]

[(1)] *Staff, Meteorological, Climatological, and Geophysical Agency (BMKG), Jakarta, Indonesia, yudhi.octantyo@gmail.com*

[(2)] *Associate Professor, Earthquake Research Institute, University of Tokyo, Tokyo, Japan, hiroe@eri.u-tokyo.ac.jp*

[(3)] *Senior Fellow, International Institute of Seismology and Earthquake Engineering, Building Research Institute, Tsukuba, Japan, tyokoi@kenken.go.jp*

Abstract

This study estimated strong motion generation area parameters and simulated the strong ground motion of the 2 August 2019 (M_w 6.9) off southwestern Java (Indonesia) intraslab earthquake and a hypothetical plate boundary earthquake (M_w 8.7) using the strong motion records of the 11 August 2019 (M_w 5.1) plate boundary earthquake with the empirical Green's function method. We first estimated the strong motion generation area that reproduced the strong ground motion during the M_w 6.9 intraslab earthquake and conducted a rough estimation of the scaling parameters to see the impact of these parameters on the performance of the synthetic waveform reproduction. We also adjusted the stress drop ratio parameter (C) for some station records, which is sensitive to waveform amplitude. Adequate synthetized waveform for the estimated strong motion generation area can be achieved for acceleration, velocity and displacement pulses. We then modeled the strong motion generation area and simulated the strong ground motion of the M_w 8.7 hypothetical plate boundary earthquake using the M_w 5.1 plate boundary earthquake and the M_w 6.9 intraslab earthquake as the element events. We tried to find the possibility of using large intraslab earthquakes that often occur inside the deeper part of the plate, to simulate the larger plate boundary earthquakes. Our estimation of the ground motion simulation for the M_w 8.7 hypothetical plate boundary earthquake was confirmed the variability in terms of source type as the element event and rupture directivity effect. The simulated ground motion was further applied in Jakarta to investigate the long-period ground motion content and identify the characteristic behavior in the synthetic waveform resulting from simulation process. We found that the long-period ground motion contents was enhanced in the application result of the empirical Green's function simulation for the M_w 8.7 hypothetical plate boundary earthquake.

Keywords: simulation, strong ground motion, empirical Green's function, long-period ground motion

1. Introduction

The Indonesia archipelago is one of the regions with the most concentrated seismic activity on the Earth. Five major tectonic plates interact within the Indonesia archipelago, in accordance with the MORVEL model [1]. One of the highest risk regions threaten by the seismic hazard is the Java island, the most populated island in Indonesia. The Java island region is overshadowed by the potencies for the next large earthquakes occurrence from the seismic activities of the off southern Java coast subduction zone. There is a possibility of seismic gap area lead by the indication of the interplate coupling activities [2] and lack of seismicity [3] with the accumulated seismic moment equivalent to a *Mw* 8.7 earthquake. It is important to understand the strong ground motion characteristic triggered by a large earthquake, to anticipate recurrence of similar or larger earthquakes. But since the available historical information of the strong ground motion is limited, strong ground motion simulation may be helpful to fulfill the requirement of earthquake engineering application as well as the seismic hazard assessment.

This study applied the empirical Green's function method formulated by [4] and [5] to perform the strong ground motion simulation for the most recent significant earthquake event of the 2 August 2019 off southwestern of Java, Indonesia, intraslab earthquake (*Mw* 6.9) utilizing strong motion recordings of the 11 August 2019 off southwestern of Java, Indonesia, plate boundary earthquake (*Mw* 5.1) as the element event. Earthquake source parameter modeling is accomplished by following the recipe formulated by [6]. We also tried to simulating strong ground motion for the maximum magnitude scenario of a plate boundary earthquake (*Mw* 8.7) in the same region, by utilizing the strong motion records of the *Mw* 5.1 plate boundary earthquake and the *Mw* 6.9 intraslab earthquake as the element events. The simulated ground motion was further applied in Jakarta, the capital city of Indonesia, to investigate the long-period ground motion content and identify the characteristic behavior in the synthetic waveform resulting from the simulation process.

2. Data

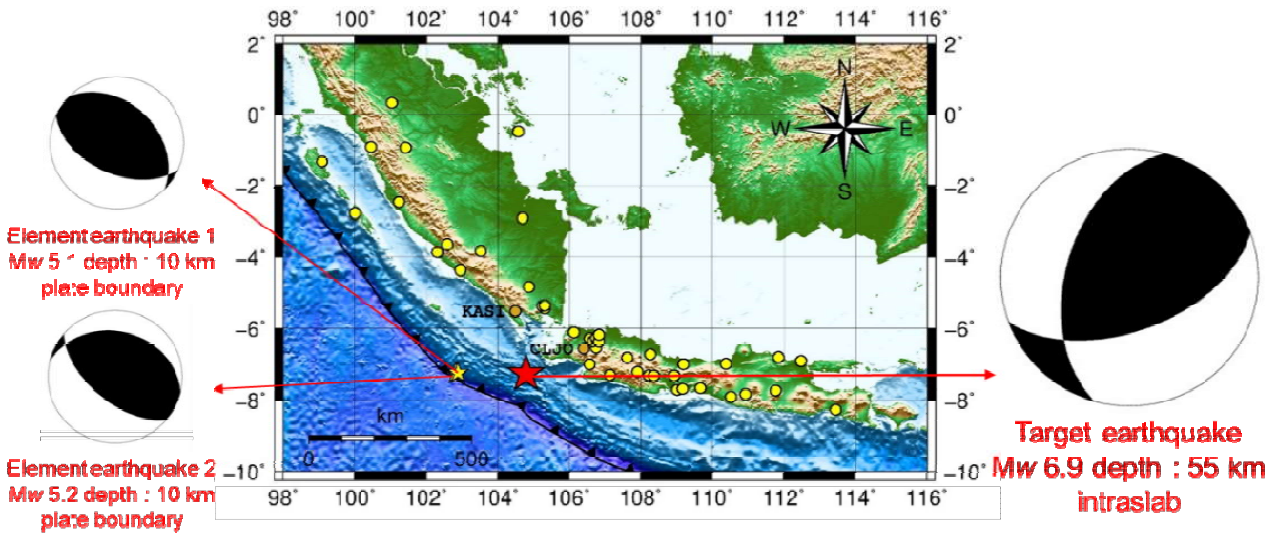

Figure 1. Hypocenters of the 2 August 2019 target earthquake along with alternative element earthquakes (parameter and focal mechanism by BMKG catalog) and the 47 recorded strong motion stations (yellow dots).

We selected the 2 August 2019 (*Mw* 6.9) intraslab earthquake as the target event for the strong ground motion simulation. However, this earthquake had a deficiency of aftershock and there is also no appropriate

event having a similar characteristic with this earthquake in adjacent area. We decided to select plate boundary earthquakes occurred on 11 August 2019 with magnitudes *Mw* 5.1 and *Mw* 5.2, as the alternative element events to simulate the target earthquake, which were recorded at many strong motion observation stations. We aware that the element events and the target event have significant differences in the distance and the focal depth, as well as the source mechanism and characteristic. This study was presented to overcome these differences in obtaining well simulated waveform of the target event. In present study we analyzed the target event which were recorded at 47 INSMN stations located in the Sumatera and Java regions as well as the couple of earthquake events that act as the alternative Green's function element event, as shown in Figure 1.

3. Methodology

This study applied the empirical Green's function method by the formulation of [4] and [5] to obtain well-performed strong ground motion simulation. This method utilized smaller event records to reproduce the ground motion simulation of a larger event, with the assumption that those small event records consolidate propagation paths and local site effects [7]. The scaling relations between the target event and the element one in the empirical Green's function formulation are described into the ratio of fault dimensions (*N*) and stress drop (*C*) parameters, which is important to determined beforehand to obtain simulation of strong ground motion. The parameters of *N* and *C* are determined by identifying the flat-level at the displacement and acceleration spectra amplitude of the two events. By the source spectral fitting, the estimation of the moment ratio of the target event to the element one event (M_0/m_0), corner frequencies of the target event (f_{cm}) and the element one (f_{ca}) are provided. The relationships among the obtained parameters with the scaling parameters of *N* and *C* are described in Equations 1, 2, and 3 as follows.

$$\frac{M_0}{m_0} = CN^3 \qquad (f \to 0) \tag{1}$$

$$\left(\frac{M_0}{m_0}\right)\left(\frac{f_{cm}}{f_{ca}}\right)^2 = CN \qquad (f \to \infty) \tag{2}$$

$$N = \frac{f_{ca}}{f_{cm}} \quad \text{and} \quad C = \left(\frac{M_0}{m_0}\right)\left(\frac{f_{cm}}{f_{ca}}\right)^3 \tag{3}$$

The target event waveform is reproduced by summing the waveforms of element events with adjustment for the difference in the slip velocity time function between the element event and the target event. The equation of summation is written as Equations 4, 5, and 6,

$$U(t) = \sum_{i=1}^{N}\sum_{j=1}^{N}\frac{r}{r_{ij}}F(t) * (C \cdot u(t)) \tag{4}$$

$$F(t) = \delta(t - t_f) + \frac{1}{n\left(1-\frac{1}{e}\right)}\sum_{k=1}^{(N-1)n}\left[\frac{1}{e^{\frac{(k-1)}{(N-1)n}}}\delta\left\{t - t_{ij} - \frac{(k-1)T}{(N-1)n}\right\}\right] \tag{5}$$

$$t_{ij} = \frac{r_{ij} - r_o}{V_s} + \frac{\xi_{ij}}{V_r} \tag{6}$$

where U(t) represents the synthetic waveform of the target event, while u(t) the observed waveform of the element event, r the epicentral distance from each recording stations, V_s refers to S-wave velocity around source area and V_r refers to rupture velocity along the fault plane, while T is the rise time of the target event, *N* and *C* are the ratio of the fault dimension and stress drop of the target event to the element one, respectively, and F(t) is the filtering (adjustment) function for the difference in the slip velocity time function.

4. Results and Discussion

4.1 Source Parameters Estimation for the 2 August 2019 (*Mw* 6.9) Earthquake

Waveform data of the target event, as well as the waveform data of the 11 August 2019 (*Mw* 5.1) earthquake and the 11 August 2019 (*Mw* 5.2) earthquake as the element events, from the CLJO and KASI stations, were used to estimate the scaling parameter of fault dimension ratio (*N*) and stress drop ratio (*C*). We conducted a rough estimation of the scaling parameters to see the impact of these parameter to the performance of the synthetic waveform reproduction. We found that the stress drop ratio (*C*) parameter is sensitive to the amplitude of the synthetic waveform estimation for this pair of earthquakes. We had to assign the stress drop ratio (*C*) parameter separately for KASI station located in the azimuth direction of 350° and other stations that located in the azimuth direction range of 41° – 91° so the simulation of the synthetic waveform can be well performed. Detailed adjusted scaling parameters value is summarized in Table 1.

Table 1. Scaling parameters of the *Mw* 6.9 target event pairs with the *Mw* 5.1 element event.

No.	scaling parameters	KASI	other stations
1	f_{cm}	0.3 Hz	0.3 Hz
2	f_{ca}	0.9 Hz	0.9 Hz
3	N	3	3
4	C	10	10
5	propagation path adjustment coefficient	1	3
6	best fit C	10	30

Figure 2 shows the schematic model of the strong motion generation area for the target event. Sub fault dimension was set to be 2.0 km in length by 2.0 km in width, with the rise time of 0.2 second. Therefore, with the fault dimension ratio (*N*) equal to 3, the strong motion generation area dimension of the target event became 6.0 km in length by 6.0 km in width, with the rise time of 0.6 second and the initial rupture starting point at sub fault at the shallowest northern end of the strong motion generation area (1, 1).

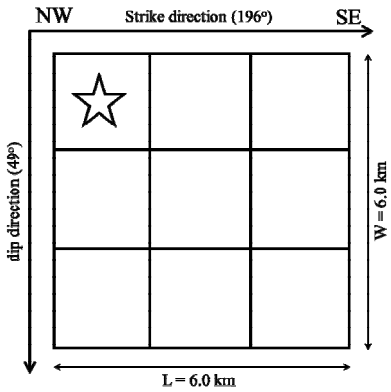

Figure 2. Strong motion generation area estimated to simulate the *Mw* 6.9 intraslab earthquake using the *Mw* 5.1 plate boundary earthquake, with fault dimension parameter, rupture starting point (star) as well as strike and dip angles.

Comparisons of the observed and synthetic waveforms for the KASI station and the CLJO station are provided in Figure 3. Here we found that through the adjustment application of the stress drop ratio (*C*), adequate synthetized waveform of the estimated strong motion generation area can be achieved for acceleration, velocity and displacement pulses recorded at the two stations.

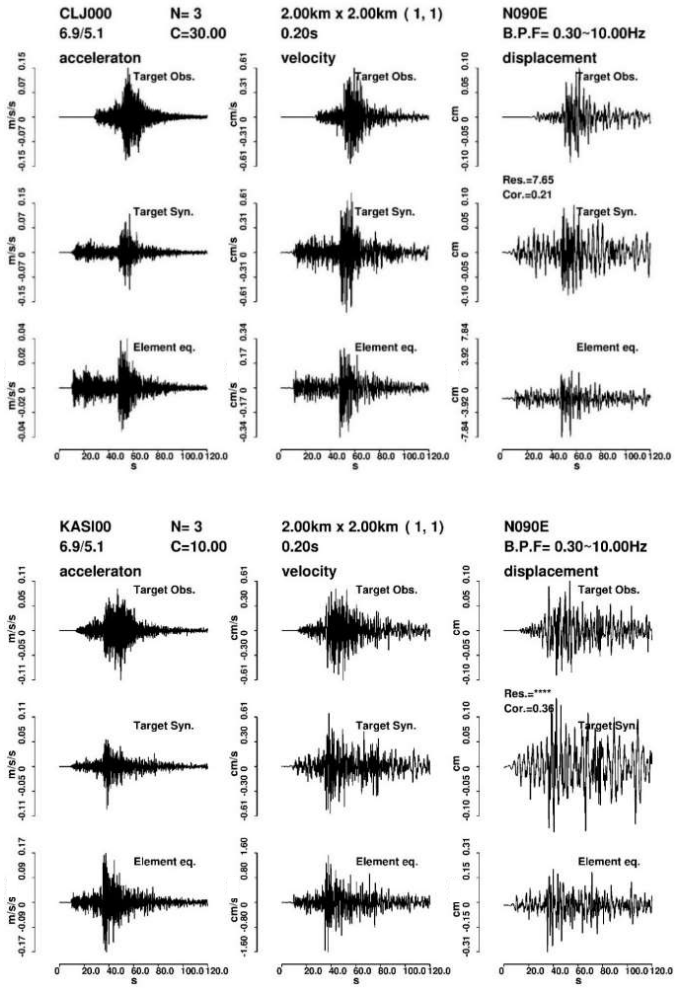

Figure 3. Ground motion simulation results of the CLJO and KASI stations (EW component).

The adjustment for the parameter of stress drop ratio (*C*) was done to prevent too large miss estimation of the synthetic waveform reproduced from the element event waveform, since we used plate boundary earthquake records as the element to synthetize the waveform of the intraslab earthquake.

The difficulty to apply only one single source parameter as the input for the ground motion simulation performance can be influenced by the factors of lateral variations, attenuation structure, or other heterogeneity of subsurface structure along the propagation path, since we have significant different in depth, fault distance and azimuth degree between the pair of earthquakes. Another factor that might be involved is the differences in the source mechanism that are assumed to have homogeneous radiation pattern due to the scale of the magnitude.

4.2 Source Parameters Estimation for the *Mw* 8.7 Hypothetical Plate Boundary Earthquake

We tried several simulations scenario for the hypothetical plate boundary earthquake with *Mw* 8.7. First simulation utilizing the plate boundary earthquake *Mw* 5.1 as the element event, with the closest sub fault from the element event hypocenter as the rupture starting point (7,1). We also tried to assign the opposite direction rupture starting point (7,5) to see the sensitivity due to rupture propagation directivity. In the first step of the first simulation, we simulated a temporary earthquake event of *Mw* 6.9; we specified the *N* parameter of 10 and *C* parameter of 1. In the second step of the first simulation, we utilized the synthetic waveform from the temporary earthquake event, as the element input for the simulation of the target hypothetical plate boundary earthquake of *Mw* 8.7. We specified the final *N* parameter of 7 in length and 5 in width with *C* parameter of 1.

Determination of *N* parameter was done using scaling relations and other supporting information from previous studies. For *C* parameter we were consistently using the value of 1 by assuming same stress drop value between target and element events, and consider the simulations as the lower bound simulations. The *C* parameter controlled the amplitude of the simulated waveform, when we assigned larger *C* parameter, we will expect larger simulated peak ground acceleration. Second simulation utilizing the intraplate earthquake *Mw* 6.9 as the element event, to find the possibility of using large intraslab earthquakes, that often occur inside the deeper part of the plate, to simulate the larger plate boundary earthquakes. Since we wanted to compare the results with the first simulation, we assigned one of the rupture starting points that is used in the first simulation, as the starting point of the second simulation. We also used the *N* and *C* parameters that already determined in the first simulation, without any adjustment. Radiation pattern correction was applied for the second simulation. The schematic illustration for the strong motion generation area of the *Mw* 8.7 hypothetical plate boundary earthquake are shown in Figures 4 and 5.

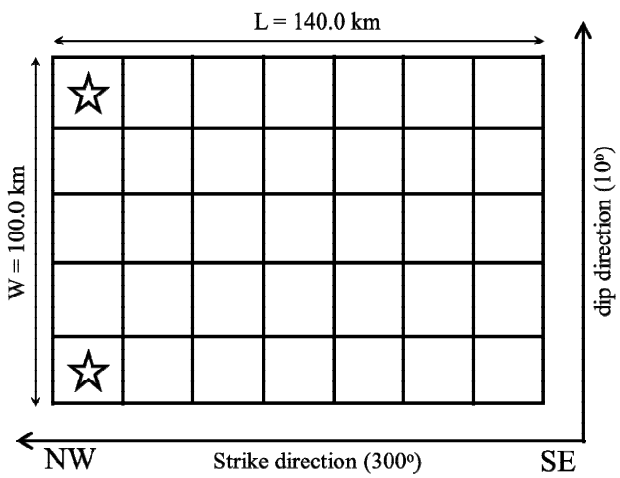

Figure 4. Strong motion generation area estimated to simulate the *Mw* 8.7 hypothetical plate boundary earthquake, with fault dimension parameter, rupture starting point (star) as well as strike and dip angles.

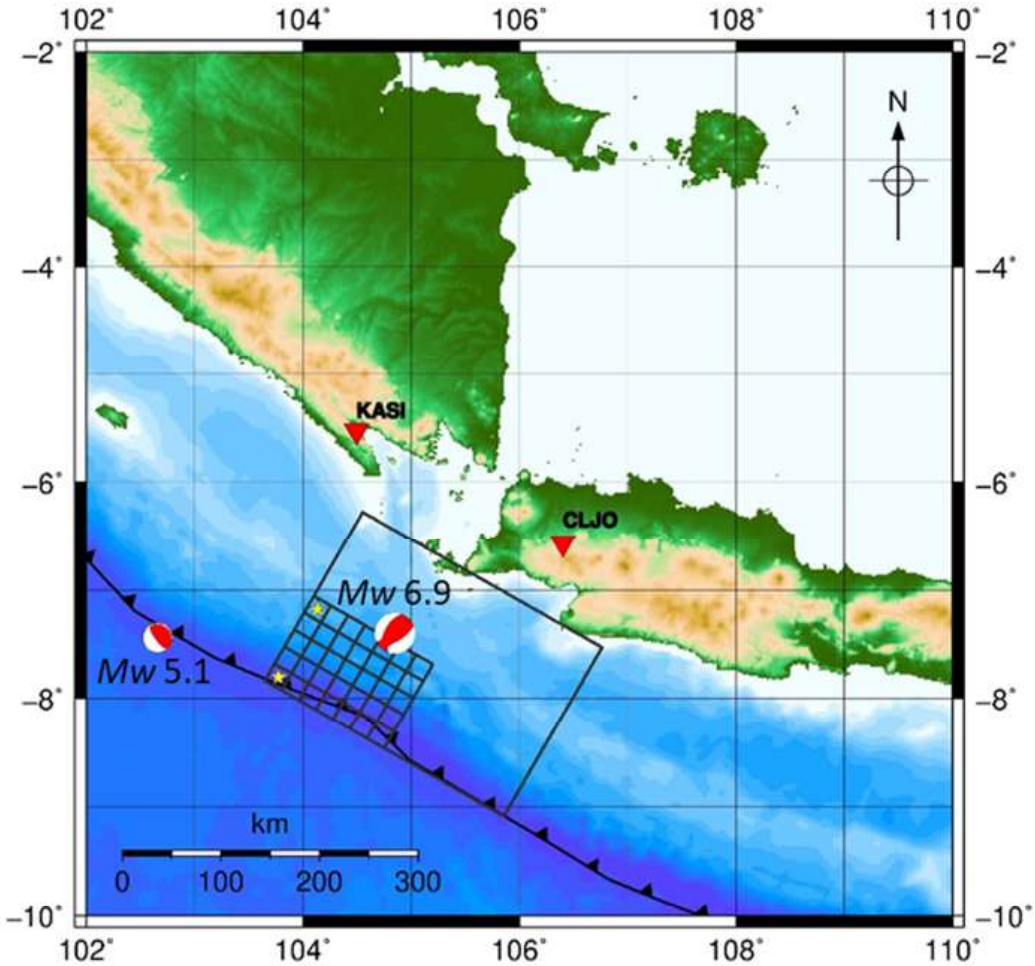

Figure 5. The *Mw* 8.7 hypothetical plate boundary earthquake simulation scheme. Large rectangle illustrates total rupture area, smaller rectangles illustrate subfaults, 7 subfaults in length by 5 subfaults in width indicate strong motion generation area. Lower yellow star is the rupture starting point subfault 7 x 1 and upper yellow star is the rupture starting point aubfault 7 x 5. Inverted triangles are the location of recording stations. Focal mechanisms represent the *Mw* 5.1 plate boundary earthquake and the *Mw* 6.9 intraslab earthquake as the element events.

4.3 Ground Motion Simulation of the *Mw* 8.7 Hypothetical Plate Boundary Earthquake Using the *Mw* 5.1 Plate Boundary Earthquake as the Element Event

We obtained well simulated acceleration waveform for the *Mw* 8.7 hypothetical plate boundary earthquake using the *Mw* 5.1 plate boundary earthquake as the element event. The first simulated acceleration waveforms were derived from the rupture starting point at subfault 7 x 1 of the strong motion generation area for a depth of 10 km, as provided in Figure 6.

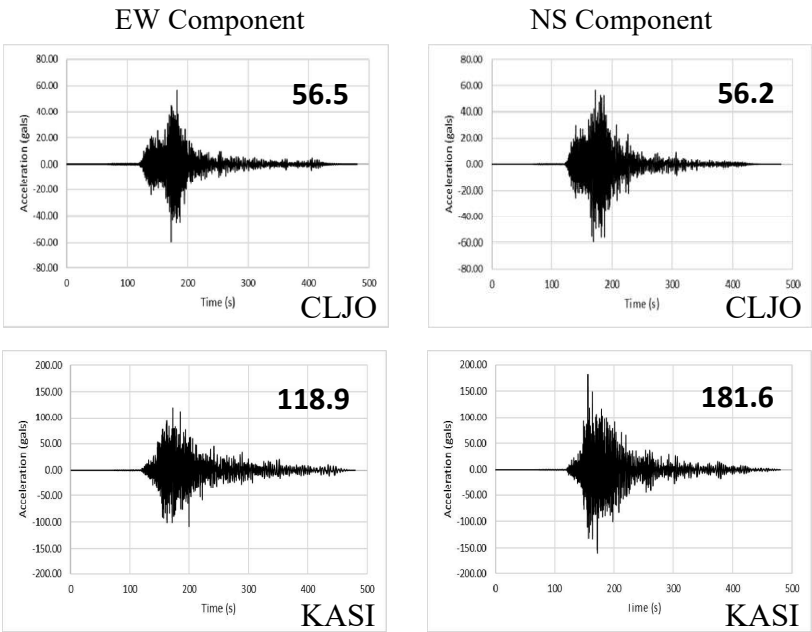

Figure 6. Simulated acceleration waveform of the *Mw* 8.7 hypothetical plate boundary earthquake at CLJO and KASI stations utilizing the *Mw* 5.1 plate boundary earthquake as the element event, with the rupture starting point at subfault 7 x 1. Peak ground acceleration in gals for each simulation is given.

The second simulated acceleration waveforms were derived from the rupture starting point at subfault 7 x 5 of the strong motion generation area for a depth of 20 km, as shown in Figure 7. We can identify that the simulation results derived from the starting point at subfault 7 x 1 have larger peak ground acceleration value compared to those derived from the starting point at subfault 7 x 5, indicating the rupture directivity effect to the earthquake ground motions in each station.

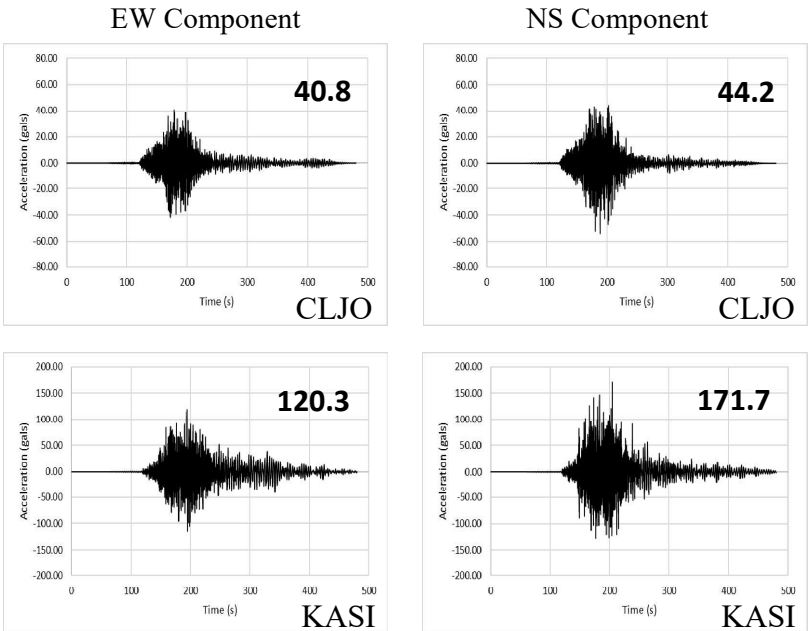

Figure 7. Simulated acceleration waveform of the *Mw* 8.7 hypothetical plate boundary earthquake at CLJO and KASI stations utilizing the *Mw* 5.1 plate boundary earthquake as the element event, with the rupture starting point at subfault 7 x 5. Peak ground acceleration in gals is given.

4.4 Ground Motion Simulation of the Mw 8.7 Hypothetical Plate Boundary Earthquake Using the Mw 6.9 Intraslab Earthquake as the Element Event

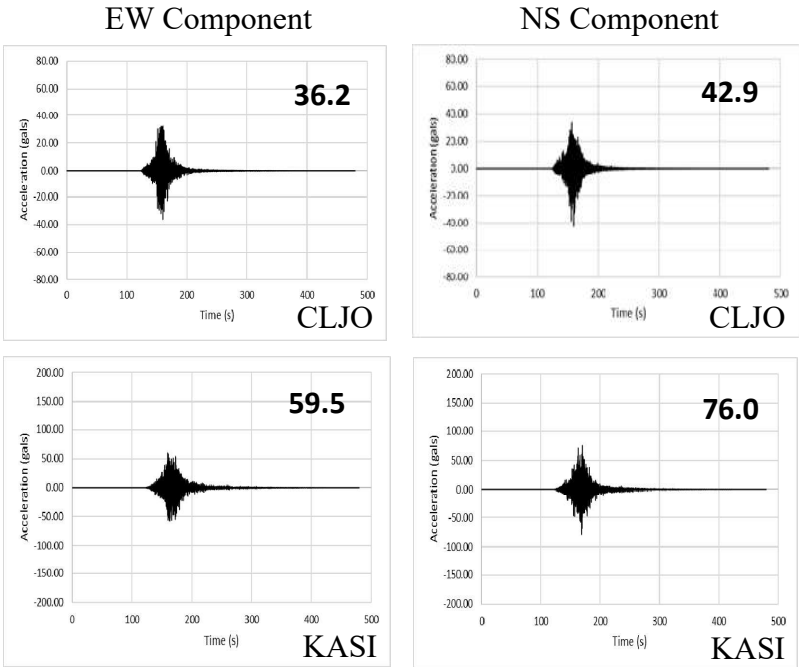

Figure 8. Simulated acceleration waveform of the *Mw* 8.7 hypothetical plate boundary earthquake at CLJO and KASI stations utilizing the *Mw* 6.9 plate boundary earthquake as the element event, with the rupture starting point at subfault 7 x 5. Peak ground acceleration in gals is given.

The simulated acceleration waveform for the *Mw* 8.7 hypothetical plate boundary earthquake using the *Mw* 6.9 intraslab earthquake as the element event for CLJO and KASI stations is shown in Figure 8. All simulations were conducted with the rupture starting point at subfault 7 x 5 of the strong motion generation area for a depth of 20 km.

The simulation results, from which utilizing the intraslab earthquake as the element event, excited smaller peak ground acceleration values compared to the simulation results which utilizing the plate boundary earthquake as the element event. Here we can assume that some source parameter adjustments might be needed to be applied, as done before for the simulation of the *Mw* 6.9 intraslab earthquake.

4.5 The Application of Simulated Ground Motion: Long-Period Ground Motion in Jakarta

We applied the simulation of the *Mw* 8.7 hypothetical plate boundary earthquake using the *Mw* 6.9 intraslab earthquake as the element event in Jakarta. Here we would like to find the long-period ground motion contents and identify the characteristic behavior in the synthetic waveform resulting from simulation process. To understand this in better way, we applied broader band pass filter ranging from 0.05 Hz to 10 Hz to the observed and simulated waveforms.

In Figure 9, we can notice from the flat level of the pseudo velocity response that the *Mw* 6.9 intraslab earthquake already contains long-period ground motion in Jakarta station ranging 0.5–7.0 seconds, and it was enhanced in the application result of the simulation for the *Mw* 8.7 hypothetical plate boundary earthquake. Nowadays, there are hundreds of 10 to 70 stories buildings in Jakarta, which generally have natural periods of 1–7 second that are vulnerable to long-period ground motion. When we compared the natural periods of these buildings with the dominant periods of the earthquakes we used in this simulation, which we can identify from the flat level of the response graphics in Figure 9, the similar periods were confirmed for both cases. This founding might mean that the high rise building in Jakarta is vulnerable for experiencing strong ground motion resonance during this kind of earthquake events.

We should note that the empirical Green's function simulation we conducted here is frequency band limited, and the simulation that derived from the intraslab earthquake as the element event tends to provide smaller PGA values, as already found in previous simulation.

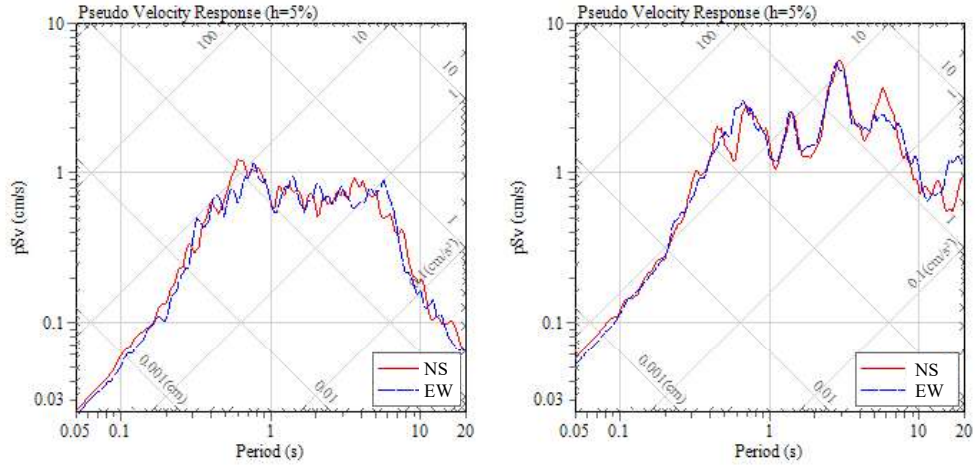

Figure 9. Comparison of the pseudo velocity response in Jakarta station between the observed *Mw* 6.9 intraslab earthquake (left figure) and the simulated *Mw* 8.7 hypothetical plate boundary earthquake (right figure).

5. Conclusions

This study utilized the empirical Green's function method to give the source parameter estimation and strong ground motion simulation of the *Mw* 6.9 intraslab earthquake located in off south-western part of the Java island using observed ground motion records of the *Mw* 5.1 plate boundary earthquake. Our study pointed that adequate synthetized waveform of a large intraslab earthquake can successfully reproduced utilizing smaller adjacent plate boundary earthquake as the element event with applying adjustment in scaling parameter. The strong ground motion level provided by the simulation was comparable to the observed peak ground acceleration values.

We also used the empirical Green's function method to simulate the acceleration level for a *Mw* 8.7 hypothetical plate boundary earthquake utilizing the *Mw* 5.1 plate boundary earthquake and the *Mw* 6.9 plate boundary earthquake as the element events. The peak ground acceleration resulted from the simulation of the *Mw* 8.7 hypothetical plate boundary earthquake simulation confirmed the variability influenced by the various type of earthquake source as the element event and the directivity effect from the designated alternatives of the rupture starting points.

The dominant periods of the earthquakes we used in this simulation were identical with the empirical natural periods of 10 to 70 stories buildings. This founding might mean that those type of buildings in Jakarta are vulnerable to the strong ground motion resonance during this kind of earthquake events. In the application of strong ground motion simulation using empirical Green's function method, fault dimension ratio parameter (*N*) and stress drop ratio parameter (*C*) become crucial control parameters for the simulation, and this is why we need to have observed target earthquake waveform, so that we can have control in our simulation result. In case of hypothetical or scenario earthquake event, where we do not have any observed record from the target earthquake, we should carefully determine the parameters. Having the supporting information regarding the parameters from previous study prior to the simulation will be helpful. Other idea is conducting trial simulations for all rupture starting points and calculate the average value of the obtained peak ground acceleration values along with the standard deviation, this idea can be conducted for future study to better fit the seismic hazard assessment.

It is important for seismologist and engineers to understand the strong ground motion characteristic triggered by a large earthquake, especially to anticipate similar or even larger events that may reoccur in the future. On the other hand, the available historical information of the strong ground motion for Indonesia region is limited, as the strong motion monitoring network has just established within the last decade. Therefore, strong ground motion simulation may be helpful to fulfill earthquake engineering application requirement, such as input time series for structural dynamics analysis. Also, providing the idea of strong ground motions for possible future earthquakes at seismically active regions can be future applied in seismic hazard assessment of the particular regions.

6. Acknowledgements

The authors would like to thank Japan International Cooperation Agency for the funding support during the completion of the study. We also acknowledge the use of strong ground motion data and earthquake catalog of the Agency for Meteorology, Climatology and Geophysics of the Republic of Indonesia. We are also grateful for the support from International Institute of Seismology and Earthquake Engineering, Building Research Institute as well as Earthquake Research Institute, University of Tokyo. Some figures were prepared using GMT and ViewWave.

7. References

[1] DeMets, C., Gordon, R. G., and Argus D.F. (2010). “Geologically current plate motions”, Geophys. J. Int., 181, 1-80.

[2] Hanifa, NR., Sagiya, T., Kimata, F., Efendi, J., Abidin, HZ., and Meilano, I. (2014). “Interplate coupling model off the southwestern coast of Java, Indonesia, based on continuous GPS data in 2008-2010” Earth Planet. Sci. Lett., 401, 159-171.

[3] National Center for Earthquake Studies of Indonesia (PUSGEN) (2017). Seismic Sources and Hazard Maps for Indonesia, Research Institute for Housing and Human Settlements, Ministry of Public Works and Housing, Republic of Indonesia.

[4] Irikura, K. (1986). “Prediction of strong acceleration motions using empirical Green’s function”, Proceedings of the 7th Japan Earthquake Engineering Symposium, 151-156.

[5] Irikura, K., and Kamae, K. (1994). “Estimation of strong ground motion in broadband-frequency band based on seismic source scaling model and empirical Green’s function technique”, Ann. Geofis, 37, 1721-1743.

[6] Miyake, H., Iwata, T., and Irikura, K. (2003). “Source characterization for broadband ground-motion simulation: Kinematic heterogeneous source model and strong motion generation area”, Bull. Seismol. Soc. Am., 93, 2531-2545.

[7] Poiata, N., and Miyake, H. (2017). “Broadband Ground Motion Simulation of the 2004 and 1977 Vrancea, Romania, Earthquakes Using Empirical Green’s Function Method”, Pure Appl. Geophys., 174, 3503-3519.

